

Modeling Femtosecond Reduction of Atomic Scattering Factors in X-ray-Excited Silicon with Boltzmann Kinetic Equations

Beata Ziaja ^{1,2,*} , Michal Stransky ^{2,3} , Konrad J. Kapcia ^{1,4}  and Ichiro Inoue ^{5,*} 

¹ Center of Free-Electron Laser Science CFEL, Deutsches Elektronen-Synchrotron DESY, Notkestr. 85, 22607 Hamburg, Germany; konrad.kapcia@amu.edu.pl

² Institute of Nuclear Physics, Polish Academy of Sciences, Radzikowskiego 152, 31-342 Kraków, Poland; michal.stransky@xfel.eu

³ European XFEL GmbH, Holzkoppel 4, 22869 Schenefeld, Germany

⁴ Institute of Spintronics and Quantum Information, Faculty of Physics, Adam Mickiewicz University in Poznań, Uniwersytetu Poznańskiego 2, 61-614 Poznań, Poland

⁵ RIKEN SPring-8 Center, 1-1-1 Kouto, Sayo 679-5148, Japan

* Correspondence: ziaja@mail.desy.de (B.Z.); inoue@spring8.or.jp (I.I.)

Abstract: In this communication, we describe the application of Boltzmann kinetic equations for modeling massive electronic excitation in a silicon nanocrystal film after its irradiation with intense femtosecond hard X-ray pulses. This analysis was inspired by an experiment recently performed at the X-ray free-electron laser facility SACLA, which measured a significant reduction in atomic scattering factors triggered by an X-ray pulse of the intensity $\sim 10^{19}$ W/cm², occurring on a timescale comparable with the X-ray pulse duration (6 fs full width at half maximum). We show that a Boltzmann kinetic equation solver can accurately follow the details of the electronic excitation in silicon atoms caused by such a hard X-ray pulse, yielding predictions in very good agreement with the experimental data.

Keywords: X-ray free-electron lasers; X-ray diffraction; computer simulations; Boltzmann kinetic equations



Citation: Ziaja, B.; Stransky, M.; Kapcia, K.J.; Inoue, I. Modeling Femtosecond Reduction of Atomic Scattering Factors in X-ray-Excited Silicon with Boltzmann Kinetic Equations. *Atoms* **2023**, *11*, 154. <https://doi.org/10.3390/atoms11120154>

Academic Editor: Luca Argenti

Received: 2 October 2023

Revised: 21 November 2023

Accepted: 24 November 2023

Published: 7 December 2023



Copyright: © 2023 by the authors. Licensee MDPI, Basel, Switzerland. This article is an open access article distributed under the terms and conditions of the Creative Commons Attribution (CC BY) license (<https://creativecommons.org/licenses/by/4.0/>).

1. Introduction

X-ray free-electron lasers (XFELs) [1–7], which produce intense X-ray pulses with femtosecond pulse durations, have stimulated the development of unique atomic-scale structure determination methods, such as protein crystallography beyond the conventional radiation dose limit [8] and visualization of ultrafast electronic and structural changes in photoinduced phase transitions [9]. In such experiments, X-rays may also act as a pump, inducing the strong excitation of electronic subsystems occurring on femtosecond timescales. Such excitation brings the matter rapidly into a strongly nonequilibrium regime (see, e.g., [10–12]), followed by a subpicosecond relaxation.

For the analysis of experimental results on X-ray-excited solid samples, in particular with application to diffraction and scattering experiments, the development of dedicated theoretical tools, capable of describing the evolution of irradiated solid materials under strongly nonequilibrium conditions, is needed. In [13], we gave a review on a robust and computationally efficient plasma simulation tool, the Boltzmann model. It is based on solving a set of Boltzmann kinetic equations for free-electron and charge-state densities present in the sample using atomistic approximation (i.e., under the assumption that the simulated sample can be initially represented as consisting of unbound atoms). Consistently, for all physical processes occurring during a sample evolution, atomic cross sections and rates are applied. This modeling approach works most accurately for the simulation of solid samples, irradiated with high-intensity X-rays. In such a case, interatomic bonds break early in the exposure, and chemical dynamics can be neglected. The Boltzmann model

can also accurately describe nonequilibrium evolution stages of an irradiated sample. This includes the treatment of atomic excitation and relaxation pathways, which can be very complicated, especially in heavy elements.

In this communication, we show that the computationally efficient Boltzmann kinetic equation code can describe the development of a massive electronic excitation in a silicon film caused by an 11.5 keV X-ray pulse with a 6 fs full-width-at-half-maximum (FWHM) duration. Its predictions on the measured diffraction signal are in very good agreement with the experimental data [1]. This confirms the strong application potential of the Boltzmann model in the hard X-ray regime due to the efficient “predominant excitation and relaxation path” (PERP) approach applied [13,14], without the need to involve a superconfiguration approach.

2. Results

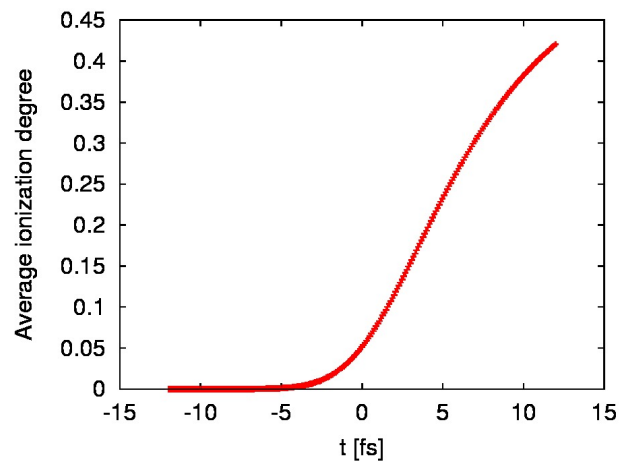
2.1. Experimental Findings

Figure 2 in Ref. [1] shows X-ray diffraction intensity profiles of silicon obtained at three high X-ray peak intensities, $\sim 2.8 \times 10^{17}$ W/cm², 3.5×10^{18} W/cm², and 4.9×10^{19} W/cm², compared with the corresponding diffraction intensity profiles at a low X-ray peak intensity, $\sim 2.1 \times 10^{16}$ W/cm². One can clearly see that the diffraction intensity profiles are similar for all X-ray intensities considered except for the peak intensity, 4.9×10^{19} W/cm². In this case, the diffraction intensity profiles obtained after the high-intensity irradiation are lower than those obtained with the reference intensity. From the diffraction intensity profiles, the diffraction efficiency can be defined as the ratio of the X-ray diffraction intensity of silicon (normalized by incident pulse energy) at a high peak intensity to that at a low peak intensity (also normalized by incident pulse energy). One can check (not shown) that for intensities of $\sim 2.8 \times 10^{17}$ W/cm² and 3.5×10^{18} W/cm², the diffraction efficiency practically does not change. On the contrary, for the highest intensity of 4.9×10^{19} W/cm², one observes a reduction of up to 40% of the diffraction efficiency. This surprising finding was analyzed in [1] with molecular dynamics calculations, using the code XMDYN [15–17].

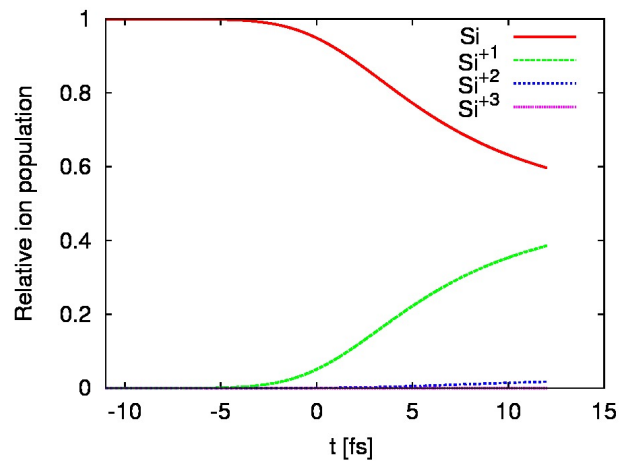
2.2. Boltzmann Code Simulations

The XMDYN code predictions shown in Figure 3b of Ref. [1] confirmed that atomic displacements even in cases with the highest X-ray peak intensity tested are negligible. The simulation predicted massive ionization (depicted in Figure 3c of Ref. [1]) and implied a femtosecond decrease in atomic form factors, resulting in a significant decrease in diffraction efficiency. XMDYN is a molecular dynamics code connected to the atomic structure calculation package XATOM [15,16]. Therefore, it can follow the evolution of all atomic configurations in the sample, calling XATOM on the fly for necessary cross sections and rates, when a specific atomic configuration appears.

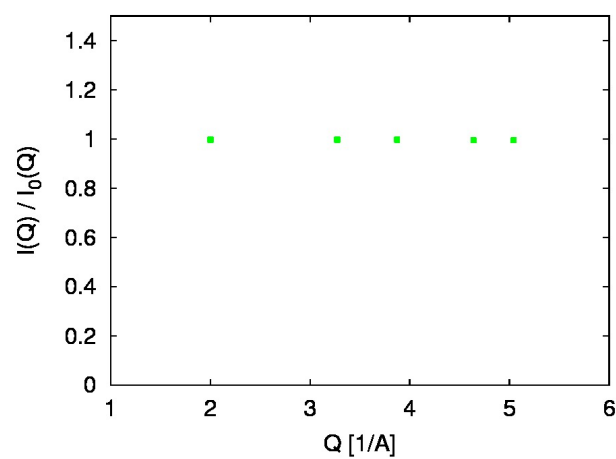
The simulation scheme is different in the Boltzmann model. Here, kinetic equations are solved for a predefined set of atomic configurations, selected using the PERP approach [13,14]. For the actual case of silicon ($Z = 14$) irradiated with 11.5 keV X-ray photons, the total number of active configurations included was 282. Charge states of up to +14 were followed. The question is how accurately such a selected set of configurations can describe the massive electron excitation going on in the sample. Figures 1–3 show the results predicted for the intensities 2.8×10^{17} W/cm², 3.5×10^{18} W/cm², and 1.0×10^{20} W/cm².



(a)

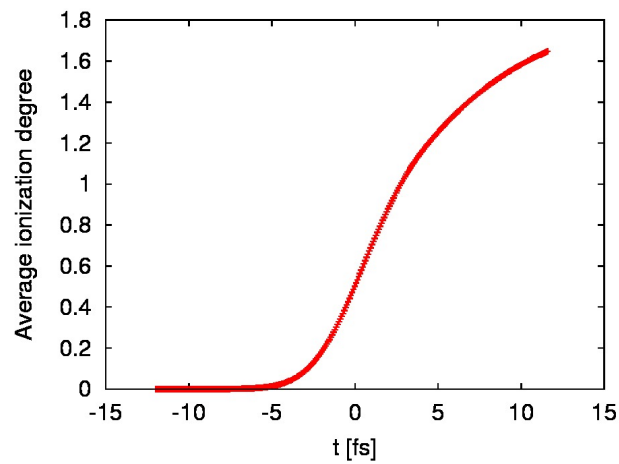


(b)

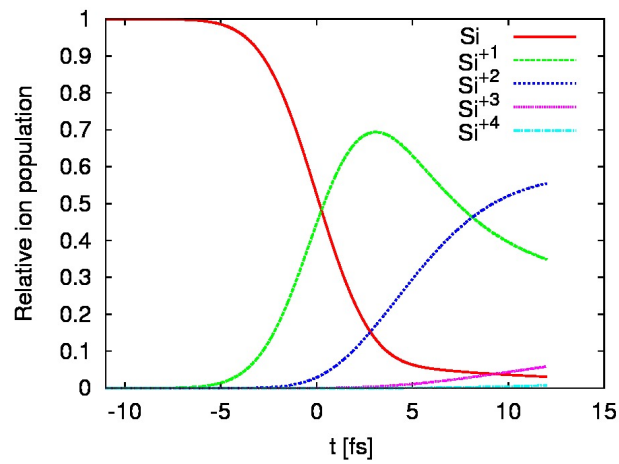


(c)

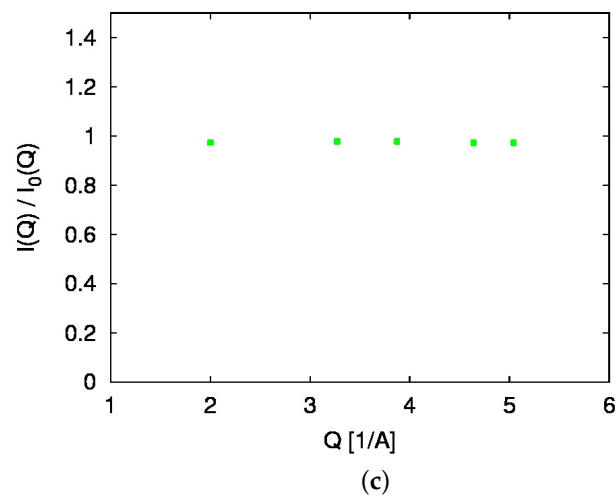
Figure 1. Predictions of the Boltzmann model for (a) the average ionization degree of silicon as a function of time, (b) relative ion populations as a function of time, and (c) diffraction efficiency for the five Bragg reflections studied in [1]. They are shown for an X-ray pulse peak intensity of $2.8 \times 10^{17} \text{ W/cm}^2$. Time zero corresponds to the maximum of an X-ray pulse (of a Gaussian temporal profile).



(a)

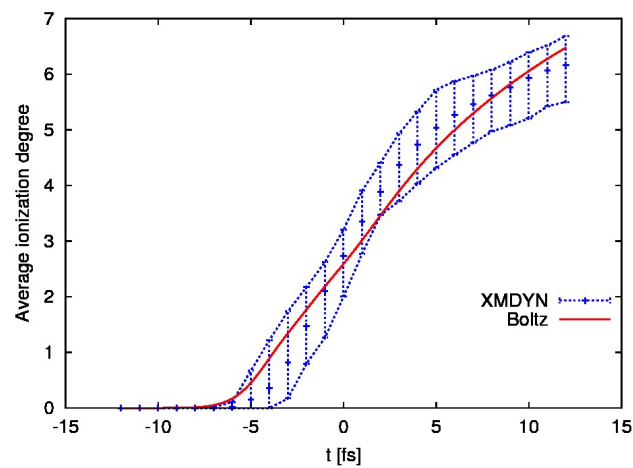


(b)

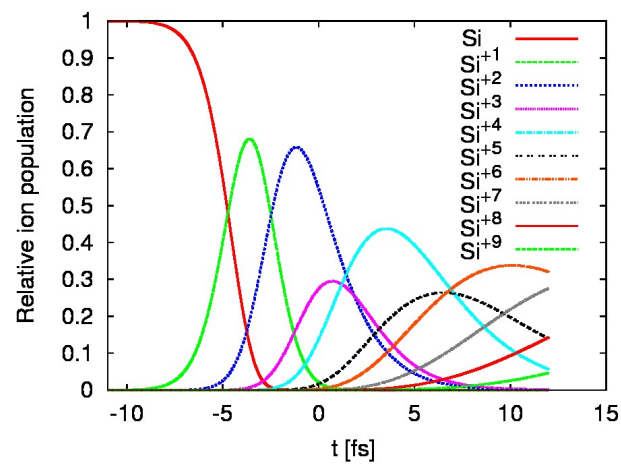


(c)

Figure 2. Predictions of the Boltzmann model for (a) the average ionization degree of silicon as a function of time, (b) relative ion populations as a function of time, and (c) diffraction efficiency for the five Bragg reflections studied in [1]. They are shown for an X-ray pulse peak intensity of $3.5 \times 10^{18} \text{ W/cm}^2$. Time zero corresponds to the maximum of an X-ray pulse (of a Gaussian temporal profile).



(a)



(b)

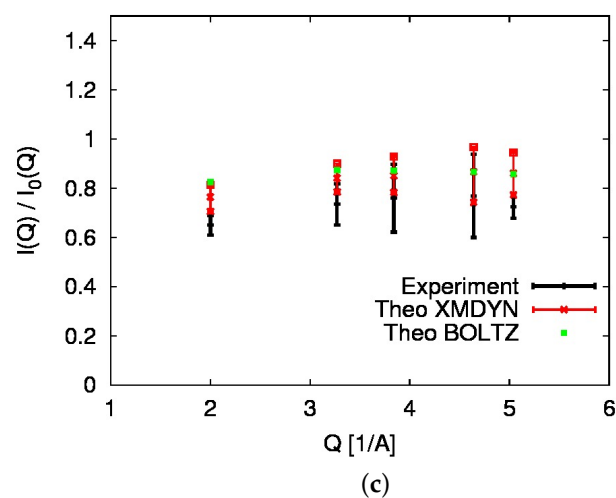


Figure 3. Predictions of the Boltzmann model for (a) the average ionization degree of silicon as a function of time, (b) relative ion populations as a function of time, and (c) diffraction efficiency for the five Bragg reflections studied in [1]. They are shown for an X-ray pulse peak intensity of $1.0 \times 10^{20} \text{ W/cm}^2$, and compared with the predictions of the XMDYN code and the experimental data from [1]. Time zero corresponds to the maximum of an X-ray pulse (of a Gaussian temporal profile).

For each X-ray peak intensity, (i) the average ionization degree of silicon as a function of time, (ii) relative charge-state populations as a function of time, and (iii) diffraction efficiency, i.e., the actual diffraction intensity, $I(Q)$, divided by the intensity, $I_0(Q)$, obtained after the irradiation of silicon with the X-ray pulse of the reference peak intensity, $2.1 \times 10^{16} \text{ W/cm}^2$, are shown. Both scattering intensities were normalized with the incident pulse energy. Note that in the simulations, we used a Gaussian temporal profile for the X-ray pulse, neglecting the spiky nature of a self-amplified spontaneous emission (SASE) XFEL pulse [18]. This problem was considered in detail in a recent publication by F. Rosmej et al. [19]. In our case, the experimental results on Bragg peak intensities presented in [1] and in Figure 3c of our manuscript are obtained after averaging the peak intensities obtained from 500 different XFEL shots [1]. The effect of the spiky pulse structure then averages out. As a shot-averaged XFEL pulse has a Gaussian temporal profile (see, e.g., Figure 1 in [18]), using the Gaussian pulse for modeling the shot-averaged data on Bragg peak intensities is justified.

In the case of two lower X-ray Bragg peak intensities, no significant change of diffraction signal is observed, in agreement with the similar diffraction intensity profiles observed in Figure 2 in Ref. [1]. The Boltzmann-model-predicted change of diffraction efficiency for the highest intensity case is in perfect agreement with the one predicted by the XMDYN code and in agreement with the experimental data. Predictions on the average charge and relative ion populations associate the change of diffraction intensity with the presence of highly charged states (up to +9) in the ionized sample. In particular, the presence of core hole states that strongly modify the diffraction properties of the sample is crucial [20]. The obtained predictions on average charge-state and transient charge-state contributions are also in very good agreement with the respective XMDYN predictions for the highest X-ray peak intensity case. This confirms the high accuracy of the Boltzmann model and its reliable applicability in the hard X-ray regime.

3. Materials and Methods

3.1. Experimental Scheme

The experiment described in Ref. [1] was performed at the XFEL facility SACLA [21,22] using a 10 μm thick silicon nanocrystal film attached to a polyimide film. The 11.5 keV X-ray pulses with a duration of 6 fs FWHM were focused with a Kirkpatrick–Baez focusing system [23] on an FWHM beam size of 180 nm (horizontal) \times 150 nm (vertical). The sample was placed at the beam focus, and five diffraction peaks (corresponding to 111, 220, 311, 400, 331 reflections) in the vertical plane were measured with a multiport charge-coupled device (MPCCD) detector [24]. The pulse energy at the sample position was monitored by a calibrated inline intensity monitor at the experimental hutch [25]. The average fluence for each pulse was determined by dividing the pulse energy by the product of horizontal and vertical beam sizes. From the average fluence, the peak intensity was derived. The diffraction intensity averaged over multiple pulses was measured for four different peak intensities: (i) $\sim 2.1 \times 10^{16} \text{ W/cm}^2$ (below damage threshold, used as reference data), (ii) $\sim 2.8 \times 10^{17} \text{ W/cm}^2$, (iii) $\sim 3.5 \times 10^{18} \text{ W/cm}^2$, and (iv) $\sim 4.9 \times 10^{19} \text{ W/cm}^2$.

3.2. Modeling Tool

Below, we briefly discuss the main components of the Boltzmann model. For further details on the code, please see the recent review paper [13] and the references therein. As mentioned above, in the Boltzmann model, the initially unexcited sample is represented as an assembly of unbound atoms. After X-ray irradiation, free electrons and various charge states appear in the sample. The continuum approach [26–28] is a computationally efficient modeling technique, well applicable in such a case. It follows ionization dynamics by solving the evolution equations for density distributions of electrons and charge states on a phase-space grid. The resulting reduction in computational costs—which now depend only on the grid size and do not scale quadratically with the number of particles, $O(N^2)$ (as typical for particle approaches, e.g., classical molecular dynamics)—is then significant.

The accurate description of the evolution of the irradiated sample also requires modeling its nonequilibrium stage, which is only possible by solving the full kinetic equations. They deliver information on the transient-electron and charge-state distributions, including various atomic configurations active during the excitation and relaxation stages in the irradiated sample.

Another modeling challenge is that highly energetic X-ray photons can release not only valence but also inner-shell electrons. They leave behind vacancies in core shells of atoms, which typically relax along very complex pathways. The relaxation occurs with the contribution of collisional processes and creates many atomic configurations. In heavier elements, a very large number of active atomic configurations involved can make the kinetic equation approach practically insolvable due to a very high computational cost, rapidly increasing with the atomic number Z . For example, in [14], we analyzed the case of carbon ($Z = 6$) irradiated by X-rays. The total number of atomic configurations was in that case equal to 27. The corresponding set of evolution equations could then be easily solved. Similarly, respective sets of kinetic equations can be formulated and solved for other light elements. However, for heavier elements, there is a strong increase in the total number of possible atomic configurations. For example, for argon ($Z = 18$), it already amounts to 1323. In order not to restrict the kinetic equation approach only to low Z elements, superconfiguration approaches were introduced (see, e.g., [29–34]). They used sets of “average” configurations [35,36] or, for spectroscopic applications, a virtual contour shape kinetic method [37], instead of treating the individual atomic configurations.

For the Boltzmann model, we proposed and tested in [14] an alternative approach to reduce the number of active atomic configurations involved in the excitation and relaxation of X-ray-irradiated materials. It is called the “predominant excitation and relaxation path” (PERP) approach, and follows the sample excitation and relaxation only along the most probable relaxation paths (including predominant photoinduced and collisional processes). This scheme, indeed, significantly restricts the number of active atomic configurations during a simulation with the Boltzmann model. In this way, computationally efficient simulations of atomic excitation and relaxation in heavier materials, such as gold [38] and copper [39], have become feasible.

Here, we applied the PERP scheme to calculate the response of a silicon sample to the impact of 11.5 keV photons, i.e., in the regime of very high photon energies, which was never tested before.

4. Discussion

We have described the implementation of the Boltzmann kinetic equations model to simulate femtosecond electron excitation in a silicon crystal during its irradiation with a 11.5 keV X-ray pulse with an FWHM duration of 6 fs. The predictions on the measured diffraction signal are in very good agreement with the experimental data and with the predictions of the MD code, XMDYN. However, both theoretical predictions systematically overestimate the experimental scattering efficiency. In order to understand the reason for that, we carefully analyzed experimental errors of X-ray pulse parameters and background subtraction. We have already included a measure of these errors in our simulations. This has improved the agreement between the simulations and the data. Still, some discrepancy has remained. The reason for this can be that the regime of very high X-ray intensities, so far poorly investigated, can bring many challenges to theoretical modeling, to mention only a possible effect of nonlinear absorption, which can manifest at such high intensities, and possible changes of atomic ionization potentials and cross sections induced by a strongly ionized and rapidly changing plasma environment. Considering all these theoretical “unknowns”, the achieved agreement between the predictions by the “low-X-ray-intensity” theory model and the experimental data can be considered very good. Of course, the development of more accurate models dedicated to a high-intensity regime is very important. The data from Ref. [1] can then be used to benchmark such models.

The simulation involved 282 active configurations, out of a total of 567 possible configurations. Charge states of up to +14 were allowed. Depending on the X-ray peak

intensity used in the simulations, the calculations took a maximum of several hours on a single CPU. This shows a strong application potential of the Boltzmann model in the hard X-ray regime, without the need to involve any superconfiguration approach.

Let us discuss the scaling of computational costs in XMDYN and the Boltzmann model in more detail. The XMDYN model is a particle approach; i.e., its computational cost increases with the squared number of particles used in the simulation. In the case of X-ray irradiation, the XMDYN simulation box should contain a sufficient number of atoms to ensure that at least several photoionization events occur in the box. For the XMDYN simulation presented in [1], when a very high X-ray fluence was applied (corresponding to X-ray peak intensities of 10^{19} – 10^{20} W/cm²), the simulation box with 64 atoms was sufficiently large. The simulation then took ~ 2 minutes on a single CPU. However, for lower X-ray fluences, the number of atoms needed for a reliable XMDYN simulation would have to be correspondingly higher. This significantly increases the computational costs when reducing the pulse fluence by a few orders of magnitude. For example, for a fluence corresponding to 10% of the above (nominal) fluence, we would need approximately 10 times as many atoms (640). The XMDYN simulation time could then be roughly estimated to ≤ 3 h. With a fluence corresponding to $\sim 1\%$ of the nominal fluence, we would need ~ 6400 atoms. This would increase the XMDYN simulation time to ≤ 14 days.

The Boltzmann code is based on the so-called continuum approach (see, e.g., [13]). In the case of bulk simulations, it does not scale with the number of atoms. Therefore, both low- and high-fluence simulation cases can be performed at a similar computational cost with the Boltzmann model, taking several hours on a single CPU for each fluence case.

Further foreseen developments, which include an improved treatment of electron–ion interaction and ionization potential lowering and implementation of Fermi–Dirac statistics for electrons [13], should remove the existing limitations of the actual Boltzmann model and transform it into a comprehensive, versatile tool for simulations of X-ray-irradiated bulk solids. The computational efficiency of the improved modeling tool is expected to be much higher than that of typical molecular dynamics approaches. The respective extensions of the Boltzmann model are already underway. Experiments necessary to validate the predictions of the extended model are being planned.

Author Contributions: Conceptualization, B.Z. and I.I.; methodology, B.Z. and M.S.; software, B.Z. and M.S.; validation, B.Z. and M.S.; investigation, B.Z., M.S., K.J.K. and I.I.; writing, all authors. All authors have read and agreed to the published version of the manuscript.

Funding: B.Z. and M.S. gratefully acknowledge the funding received from an R&D grant of the European XFEL, with the contribution of IFJ PAN in Kraków. K.J.K. thanks the Polish National Agency for Academic Exchange for the funding in the frame of the Bekker Programme (PPN/BEK/2020/1/00184).

Data Availability Statement: The data presented in this study are available on request from the corresponding author. The data are not publicly available due to licensing restrictions.

Acknowledgments: The authors thank Zoltan Jurek and Victor Tkachenko for the helpful discussions.

Conflicts of Interest: Author Michal Stransky was employed by the company European XFEL GmbH. The remaining authors declare that the research was conducted in the absence of any commercial or financial relationships that could be construed as a potential conflict of interest.

Abbreviations

The following abbreviations are used in this manuscript:

XFEL	X-ray free-electron laser
SACLA	SPring-8 Angstrom Compact free electron LAser
XMDYN	molecular-dynamics- and Monte-Carlo-based code for modeling X-ray-driven dynamics in complex systems
XATOM	atomic structure calculation tool

MD	molecular dynamics
FWHM	full width at half maximum
PERP	predominant excitation and relaxation path
MPCCD	multiport charge-coupled device
SASE	self-amplified spontaneous emission

References

- Inoue, I.; Yamada, J.; Kapcia, K.J.; Stransky, M.; Tkachenko, V.; Jurek, Z.; Inoue, T.; Osaka, T.; Inubushi, Y.; Ito, A.; et al. Femtosecond reduction of atomic scattering factors triggered by intense x-ray pulse. *Phys. Rev. Lett.* **2023**, *131*, 163201. [[CrossRef](#)]
- Lee, R.W.; Moon, S.J.; Chung, H.K.; Rozmus, W.; Baldis, H.A.; Gregori, G.; Cauble, R.C.; Landen, O.L.; Wark, J.S.; Ng, A.; et al. Finite temperature dense matter studies on next-generation light sources. *J. Opt. Soc. Am. B* **2003**, *20*, 770–778. [[CrossRef](#)]
- Ackermann, W.; Asova, G.; Ayzvazyan, V.; Azima, A.; Baboi, N.; Bähr, J.; Balandin, V.; Beutner, B.; Brandt, A.; Bolzmann, A.; et al. Operation of a free-electron laser from the extreme ultraviolet to the water window. *Nat. Photonics* **2007**, *1*, 336–342. [[CrossRef](#)]
- Allaria, E.; Appio, R.; Badano, L.; Barletta, W.A.; Bassanese, S.; Biedron, S.G.; Borga, A.; Busetto, E.; Castronovo, D.; Cinquegrana, P.; et al. Highly coherent and stable pulses from the FERMI seeded free-electron laser in the extreme ultraviolet. *Nat. Photonics* **2012**, *6*, 699–704. [[CrossRef](#)]
- Emma, P.; Akre, R.; Arthur, J.; Bionta, R.; Bostedt, C.; Bozek, J.; Brachmann, A.; Bucksbaum, P.; Coffee, R.; Decker, F.J.; et al. First lasing and operation of an Ångström-wavelength free-electron laser. *Nat. Photonics* **2010**, *4*, 641–647. [[CrossRef](#)]
- Pile, D. First light from SACLA. *Nat. Photonics* **2011**, *5*, 456–457. [[CrossRef](#)]
- Weise, H.; Decking, W. Commissioning and first lasing of the European XFEL. In Proceedings of the 38th International Free Electron Laser Conference FEL2017, Santa Fe, NM, USA, 20–25 August 2017; pp. 9–13. [[CrossRef](#)]
- Chapman, H.N.; Caleman, C.; Timneanu, N. Diffraction before destruction. *Philos. Trans. R. Soc. B* **2014**, *369*, 20130313. [[CrossRef](#)]
- Lindenberg, A.M.; Johnson, S.L.; Reis, D.A. Visualization of Atomic-Scale Motions in Materials via Femtosecond X-Ray Scattering Techniques. *Ann. Rev. Mat. Res.* **2017**, *47*, 425–449. [[CrossRef](#)]
- Gorkhover, T.; Adolph, M.; Rupp, D.; Schorb, S.; Epp, S.W.; Erk, B.; Foucar, L.; Hartmann, R.; Kimmel, N.; Kühnel, K.U.; et al. Nanoplasma Dynamics of Single Large Xenon Clusters Irradiated with Superintense X-Ray Pulses from the Linac Coherent Light Source Free-Electron Laser. *Phys. Rev. Lett.* **2012**, *108*, 245005. [[CrossRef](#)] [[PubMed](#)]
- Tachibana, T.; Jurek, Z.; Fukuzawa, H.; Motomura, K.; Nagaya, K.; Wada, S.; Johnsson, P.; Siano, M.; Mondal, S.; Ito, Y.; et al. Nanoplasma Formation by High Intensity Hard X-rays. *Sci. Rep.* **2015**, *5*, 10977. [[CrossRef](#)] [[PubMed](#)]
- Inoue, I.; Deguchi, Y.; Ziaja, B.; Osaka, T.; Abdullh, M.M.; Jurek, Z.; Medvedev, N.; Tkachenko, V.; Inubushi, Y.; Kasai, H.; et al. Atomic-Scale Visualization of Ultrafast Bond Breaking in X-Ray-Excited Diamond. *Phys. Rev. Lett.* **2021**, *126*, 117403. [[CrossRef](#)] [[PubMed](#)]
- Ziaja, B.; Bekx, J.J.; Masek, M.; Medvedev, N.; Lipp, V.; Saxena, V.; Stransky, M. Application of Boltzmann kinetic equations to model X-ray-created warm dense matter and plasma. *Philos. Trans. R. Soc. A* **2023**, *381*, 20220216. [[CrossRef](#)] [[PubMed](#)]
- Ziaja, B.; Saxena, V.; Son, S.K.; Medvedev, N.; Barbrel, B.; Woloncewicz, B.; Stransky, M. Kinetic Boltzmann approach adapted for modeling highly ionized matter created by x-ray irradiation of a solid. *Phys. Rev. E* **2016**, *93*, 053210. [[CrossRef](#)] [[PubMed](#)]
- Son, S.K.; Young, L.; Santra, R. Impact of hollow-atom formation on coherent x-ray scattering at high intensity. *Phys. Rev. A* **2011**, *83*, 033402. [[CrossRef](#)]
- Jurek, Z.; Son, S.K.; Ziaja, B.; Santra, R. XMDYN and XATOM: Versatile simulation tools for quantitative modeling of X-ray free-electron laser induced dynamics of matter. *J. Appl. Crystallogr.* **2016**, *49*, 1048–1056. [[CrossRef](#)]
- Murphy, B.F.; Osipov, T.; Jurek, Z.; Fang, L.; Son, S.K.; Mucke, M.; Eland, J.H.D.; Zhaunerchyk, V.; Feifel, R.; Avaldi, L.; et al. Femtosecond X-ray-induced explosion of C60 at extreme intensity. *Nat. Commun.* **2014**, *5*, 4281. [[CrossRef](#)]
- Duesterer, S.; Hartmann, G.; Bomme, C.; Boll, R.; Costello, J.T.; Erk, B.; De Fanis, A.; Ilchen, M.; Johnsson, P.; Kelly, T.J.; et al. Two-color XUV+NIR femtosecond photoionization of neon in the near-threshold region. *New J. Phys.* **2019**, *21*, 063034. [[CrossRef](#)]
- Rosmej, F.B.; Astapenko, V.A.; Khramov, E.S. XFEL and HHG interaction with matter: Effects of ultrashort pulses and random spikes. *Matter Radiat. Extrem.* **2021**, *6*, 034001. [[CrossRef](#)]
- Als-Nielsen, J.; McMorrow, D. *Elements of Modern X-ray Physics*; John Wiley and Sons: Hoboken, NJ, USA, 2011.
- Yabashi, M.; Tanaka, H.; Ishikawa, T. Overview of the SACLA facility. *J. Synchrotron Radiat.* **2015**, *22*, 477–484. [[CrossRef](#)]
- Tono, K.; Togashi, T.; Inubushi, Y.; Katayama, T.; Owada, S.; Yabuuchi, T.; Kon, A.; Inoue, I.; Osaka, T.; Yumoto, H.; et al. Overview of optics, photon diagnostics and experimental instruments at SACLA: Development, operation and scientific applications. In Proceedings of the SPIE Advances in X-ray Free-Electron Lasers Instrumentation IV, Prague, Czech Republic, 26–28 April 2017; Tschentscher, T., Patthey, L., Eds.; International Society for Optics and Photonics: Prague, Czech Republic, 2017; Volume 10237, pp. 1–10. [[CrossRef](#)]
- Yumoto, H.; Inubushi, Y.; Osaka, T.; Inoue, I.; Koyama, T.; Tono, K.; Yabashi, M.; Ohashi, H. Nanofocusing Optics for an X-Ray Free-Electron Laser Generating an Extreme Intensity of 100 EW/cm² Using Total Reflection Mirrors. *Appl. Sci.* **2020**, *10*, 2611. [[CrossRef](#)]
- Kameshima, T.; Ono, S.; Kudo, T.; Ozaki, K.; Kirihara, Y.; Kobayashi, K.; Inubushi, Y.; Yabashi, M.; Horigome, T.; Holland, A.; et al. Development of an X-ray pixel detector with multi-port charge-coupled device for X-ray free-electron laser experiments. *Rev. Sci. Instrum.* **2014**, *85*, 033110. [[CrossRef](#)] [[PubMed](#)]

25. Tono, K.; Togashi, T.; Inubushi, Y.; Sato, T.; Katayama, T.; Ogawa, K.; Ohashi, H.; Kimura, H.; Takahashi, S.; Takeshita, K.; et al. Beamline, experimental stations and photon beam diagnostics for the hard x-ray free electron laser of SACLA. *New J. Phys.* **2013**, *15*, 083035. [[CrossRef](#)]
26. Ethier, S.; Matte, J.P. Electron kinetic simulations of solid density Al plasmas produced by intense subpicosecond laser pulses. I. Ionization dynamics in 30 femtosecond pulses. *Phys. Plasmas* **2001**, *8*, 1650–1658. [[CrossRef](#)]
27. Ziaja, B.; de Castro, A.R.B.; Weckert, E.; Moeller, T. Modelling dynamics of samples exposed to free-electron-laser radiation with Boltzmann equations. *Eur. Phys. J. D* **2006**, *40*, 465–480. [[CrossRef](#)]
28. Sherlock, M.; Hill, E.G.; Rose, S.J. Kinetic simulations of the heating of solid density plasma by femtosecond laser pulses. *High Eng. Density Phys.* **2013**, *9*, 38–41. [[CrossRef](#)]
29. Bar-Shalom, A.; Oreg, J.; Goldstein, W.H.; Shvarts, D.; Zigler, A. Super-transition-arrays: A model for the spectral analysis of hot, dense plasma. *Phys. Rev. A* **1989**, *40*, 3183–3193. [[CrossRef](#)]
30. Oreg, J.; Bar-Shalom, A.; Klapisch, M. Operator technique for calculating superconfiguration-averaged quantities of atoms in plasmas. *Phys. Rev. E* **1997**, *55*, 5874–5882. [[CrossRef](#)]
31. Chung, H.K.; Chen, M.; Morgan, W.; Ralchenko, Y.; Lee, R. FLYCHK: Generalized population kinetics and spectral model for rapid spectroscopic analysis for all elements. *High Eng. Density Phys.* **2005**, *1*, 3–12. [[CrossRef](#)]
32. Peyrusse, O.; Bauche-Arnoult, C.; Bauche, J. Effective superconfiguration temperature and the radiative properties of nonlocal thermodynamical equilibrium hot dense plasma. *Phys. Plasmas* **2005**, *12*, 063302. [[CrossRef](#)]
33. Abdallah, J.; Sherrill, M.; Kilcrease, D.; Fontes, C.; Zhang, H.; Oelgoetz, J. The reduced detailed configuration accounting (RDCA) model for NLTE plasma spectral calculations. *High Eng. Density Phys.* **2009**, *5*, 204–207. [[CrossRef](#)]
34. Bauche, J.; Bauche-Arnoult, C.; Peyrusse, O. Superconfigurations and Super Transition Arrays. In *Atomic Properties in Hot Plasmas: From Levels to Superconfigurations*; Springer International Publishing: Cham, Switzerland, 2015; pp. 203–223. [[CrossRef](#)]
35. Lee, Y.T. A model for ionization balance and L-shell spectroscopy of non-LTE plasmas. *J. Quant. Spectr. Radiat. Trans.* **1987**, *38*, 131–145. [[CrossRef](#)]
36. Marchand, R.; Caillé, S.; Lee, Y. Improved screening coefficients for the hydrogenic ion model. *J. Quant. Spectr. Radiat. Trans.* **1990**, *43*, 149–154. [[CrossRef](#)]
37. Rosmej, F.B. An alternative method to determine atomic radiative emission. *Europhys. Lett.* **2006**, *76*, 1081–1087. [[CrossRef](#)]
38. Ziaja, B.; Bekx, J.J.; Masek, M.; Medvedev, N.; Piekarz, P.; Saxena, V.; Stransky, M.; Toleikis, S. Tracing X-ray-induced formation of warm dense gold with Boltzmann kinetic equations. *Eur. Phys. J. D* **2021**, *75*, 224. [[CrossRef](#)]
39. Mercadier, L.; Benediktovitch, A.; Krusic, S.; Schlappa, J.; Agåker, M.; Carley, R.; Fazio, G.; Gerasimova, N.; Kim, Y.Y.; Le Guyader, L.; et al. Transient Absorption of Warm Dense Matter Created by an X-Ray Free-Electron Laser. *Res. Sq.* **2023**, preprint.

Disclaimer/Publisher’s Note: The statements, opinions and data contained in all publications are solely those of the individual author(s) and contributor(s) and not of MDPI and/or the editor(s). MDPI and/or the editor(s) disclaim responsibility for any injury to people or property resulting from any ideas, methods, instructions or products referred to in the content.